International Journal of Cardiology 222 (2016) 202–208

Contents lists available at ScienceDirect

International Journal of Cardiology

journal homepage: www.elsevier.com/locate/ijcard

# Impact of catheter tip-tissue contact on three-dimensional left atrial geometries: Relationship between the external structures and anatomic distortion of 3D fast anatomical mapping and high contact force guided images

Naofumi Anjo MD [a], Shiro Nakahara MD [a,*], Yasuo Okumura MD [b], Yuichi Hori MD [a], Koichi Nagashima MD [b], Takaaki Komatsu MD [a], Akiko Hayashi MD [a], Sayuki Kobayashi MD [a], Yoshihiko Sakai MD [a], Isao Taguchi MD [a]

[a] Department of Cardiology, Dokkyo Medical University Koshigaya Hospital, Saitama, Japan
[b] Division of Cardiology, Department of Medicine, Nihon University School of Medicine, Tokyo, Japan

ARTICLE INFO

*Article history:*
Received 13 June 2016
Accepted 27 July 2016
Available online 28 July 2016

*Keywords:*
Catheter ablation
Atrial fibrillation
Contact force

ABSTRACT

*Background:* A high catheter tip-tissue contact force (CF) with the myocardium may cause 3-dimensional (3D) map distortion, however, the influence of external structures surrounding the left atrium (LA) on that distortion remains unknown. This study characterized the impact of high CF mapping on the local LA geometry distortion.
*Methods:* Thirty AF patients underwent 3D-ultrasound merged with CT images (3D-Merge-CT). The LA area in contact with external structures was identified by enhanced CT. Fast-electroanatomical-mapping (FAM) geometries were created by two methods, point-by-point mapping with high (>10 g) CFs (high-CF guided-FAM), followed by that with multielectrode-mapping catheters (conventional-FAM). The resulting geometries were compared with the 3D-Merge-CT images.
*Results:* Three representative anatomical contact areas (ascending aorta-vs.-anterior wall, descending aorta-vs.-left pulmonary vein [PV], and vertebrae-vs.-posterior wall) were identified. The PV antrum distorted distance on the 3D-Merge-CT was significantly longer for high-CF guided-FAMs than conventional-FAMs (1.7[0–3.6] vs. 0[0–1.8]mm, $P < 0.0001$). In high-CF maps, the distorted distance significantly differed between regions with and without contact areas in both the PV antrum (0[0–0.17] vs. 1.7[0–3.9]mm, $P = 0.0201$) and LA body region (0[0–1.5] vs. 1.7[0.7–2.2]mm, $P < 0.005$). The catheter tip-tissue CF did not correlate with the distorted distance ($r = 0.08$, $P = 0.46$), and a multivariate analysis revealed that the absence of anatomical contact areas was strongly associated with significant local distortion, independent of the CF.
*Conclusions:* High-CF guided mapping yields greater 3D-image anatomical distortion than conventional-FAM methods. That distortion was attenuated by regions with anatomical contact areas, suggesting that regional anatomic distortion is involved in the existence of external structures surrounding the LA.


## 1. Introduction

Recent advancement in ablation and mapping technologies has enabled real-time contact force (CF) monitoring during procedures. Prior studies have shown that the CF is one of the important determinants for the radiofrequency (RF) ablation lesion size [1]. A high CF against the myocardium may cause 3-dimensional (3D) map distortion and the left atrial (LA) geometry created on 3D mapping systems significantly differs when the map is created with different CFs [2]. However, up to now, the influence of external structures surrounding the left atrium (LA) on that distortion remains unknown. The present study aimed to characterize the impact of high CF mapping on the local anatomical distortion of the LA geometry in patients with atrial fibrillation (AF).

## 2. Methods

### 2.1. Study patients

The subjects consisted of 30 patients with symptomatic drug refractory paroxysmal AF who were referred to Dokkyo Medical University Koshigaya Hospital for RF catheter ablation. The clinical characteristics are shown in Table 1. Adequate oral anticoagulation was given for at least 1 month before the procedure. Upon admission, transesophageal and transthoracic echocardiograms were obtained. All patients gave their written informed consent. The study protocol was approved by the hospital's institutional review board. The study complied with the Declaration of Helsinki.

* Corresponding author at: Department of Cardiology, Dokkyo University Koshigaya Hospital, 2-1-50 Minami Koshigaya, Koshigaya, Saitama 343–8555, Japan.
*E-mail address:* nshiro@dokkyomed.ac.jp (S. Nakahara).

http://dx.doi.org/10.1016/j.ijcard.2016.07.186
0167-5273/

**Table 1**
Patient characteristics.

| | Study subjects (n = 30) |
|---|---|
| Age (years) | 64 ± 8 |
| Gender (male/female) | 16/14 |
| Duration of AF (month) | 24 (12–69) |
| Hypertension | 18 (60) |
| Diabetes mellitus | 3 (10) |
| Heart failure | 1 (3) |
| Stroke | 1 (3) |
| Left atrial diameter (mm) | 38 ± 5 |
| Left ventricular ejection fraction | 68 ± 6 |

The values are expressed as the mean ± SD, median and interquartile range, or n (%). AF = atrial fibrillation.

### 2.2. Computed tomography imaging and image segmentation

One day before the procedure, multidetector helical computed tomography (CT) (64-channel Somatom-Definition; Siemens-Medical Solutions, Forchheim, Germany) was performed. All patients demonstrated sinus rhythm (SR) at the time of the CT imaging. During the end-expiratory phase, volume image acquisitions were gated at the P wave of ECG lead II. Segmented images of the LA with all pulmonary veins (PVs) derived from chamber volume data were used to reconstruct the structures by means of a 3-step process described previously [3,4].

### 2.3. Cardiac catheterization

The electrophysiological procedure was performed while patients were in the fasting state. With patients under local anesthesia, a 10 Fr SoundStar ultrasound catheter (Biosense Webster, Diamond Bar, CA) was inserted into the right atrium via the right femoral vein, and anatomic mapping of the LA by the CartoSound module equipped in a CARTO3 system (Biosense Webster) was performed. After the transseptal puncture was performed, 5000 units of heparin was injected into the LA, followed by repetitive injections of 1000 to 2000 units of heparin to maintain an activated clotting time ≥300 s during the procedure. All procedures were performed by 1 operator (N.A.), who had performed over 1000 PV isolation procedures. Two 8.5 Fr long sheaths (Swartz SL1, St. Jude Medical, St. Paul, MN) were inserted into the LA, and no steerable sheath was used in this study.

### 2.4. 3D-CT merge process

Intracardiac echocardiography (ICE) images were displayed through the CartoSound module using an Acuson X300PE echocardiography system (Siemens Medical Solutions USA, Mountain View, CA). ICE plane images were obtained at the end-tidal position (ACCURESP, Biosense Webster) and 50% of the R-R interval as described previously [5]. The range of the contours sampled was 6 to 9 between the ostia of the right PV and left PV, and these contours were registered as the LA ICE image. After visual alignment, the 2 images were integrated with the installed surface registration program [6].

### 2.5. Creation of a conventional fast-electroanatomical-mapping (FAM) and high-CF guided FAM

After the 3D-CT merge process, 3D geometries of the LA and PVs were created with an FAM algorithm [7,8]. In brief, high-resolution 3D chamber volumes were created from continuous recordings of the multipolar catheter movements within the cardiac chambers to outline the structures. All geometries were created during SR, and the 3D geometries were automatically gated to the respirations (ACCURESP), and the FAM and mapping points for the analysis were acquired during the expiration phase. Regarding the creation of the conventional-FAM, the ablation catheter was only used for verification of each PV location, and a 20-pole multielectrode steerable mapping catheter arranged with 5 soft radiating splines covering a diameter of 3.5 cm (Pentaray, Biosense Webster) was used for the LA geometry. A typical example of a conventional-FAM geometry is demonstrated in Fig. 1 (left panel).

In order to characterize the regional distortion area of the LA, point-by-point mapping with a high (>10 g) contact force at each PV antrum and the LA body surface were created (high-CF guided FAM) after the creation of the conventional FAM. The operators tried to keep a certain level of high contact (10–50 g) at each mapping point. No radiofrequency applications were delivered during the creation of high-CF guided FAM. A typical example of a conventional-FAM geometry is demonstrated in Fig. 1 (right panel). Systematic high-CF guided PV antrum maps in each of the 8 segments of the left and right PVs were created (Fig. 2A).

The LA shell was also divided into 6 distinct anatomic segments [9]: septum, anterior wall, floor, lateral wall, posterior wall, and roof in that order (Fig. 3A). High-CF guided points were systematically obtained with at least 2 points in each segmented PV antral region, and at least 3 points (>5 mm separation from each other) in each LA region.

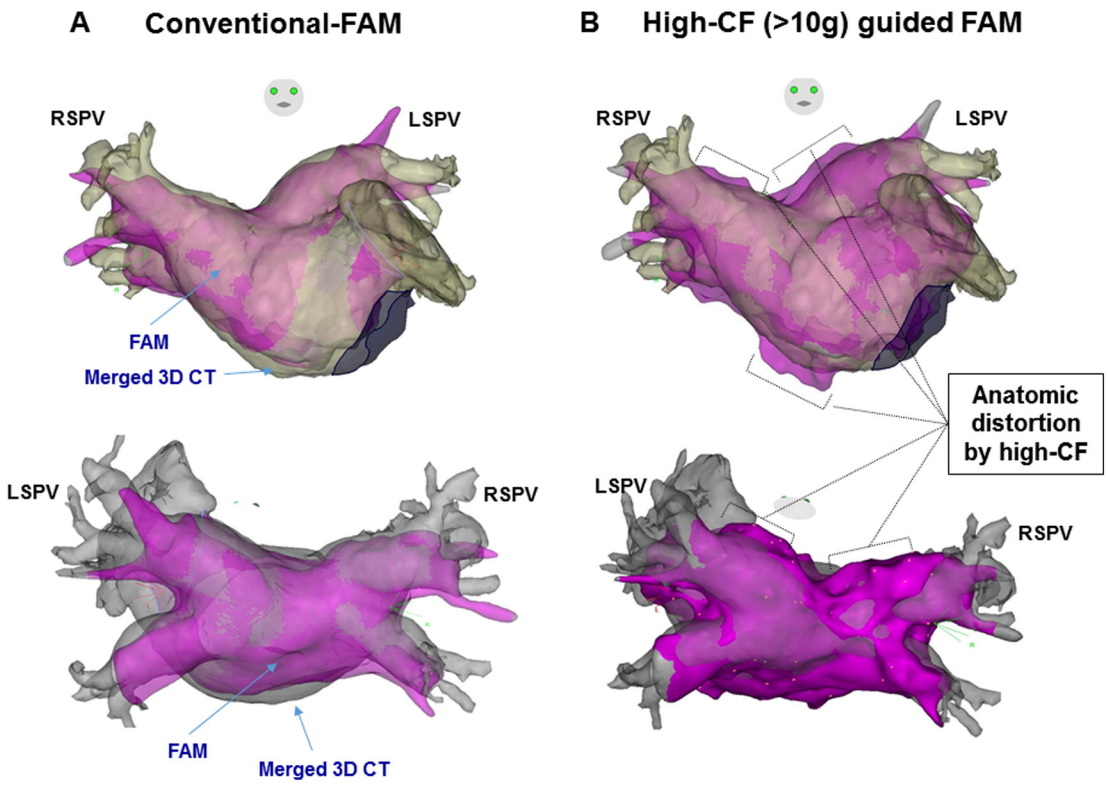


**Fig. 1.** A: Typical example of merged 3D US-CT-derived and conventional FAM-derived geometries. B: Typical example of merged 3D US-CT-derived and high contact force (>10 g) guided FAM-derived geometries. A large difference in the distance from the 3D US-derived rendering was noted between the conventional FAM-derived rendering and high contact force (>10 g) guided FAM-derived rendering at the roof of both the right and left PV antra, roof, septum, and floor of the left atrial body region. FAM, fast anatomical mapping; vein; LSPV, left superior pulmonary vein, RSPV, right superior pulmonary vein.

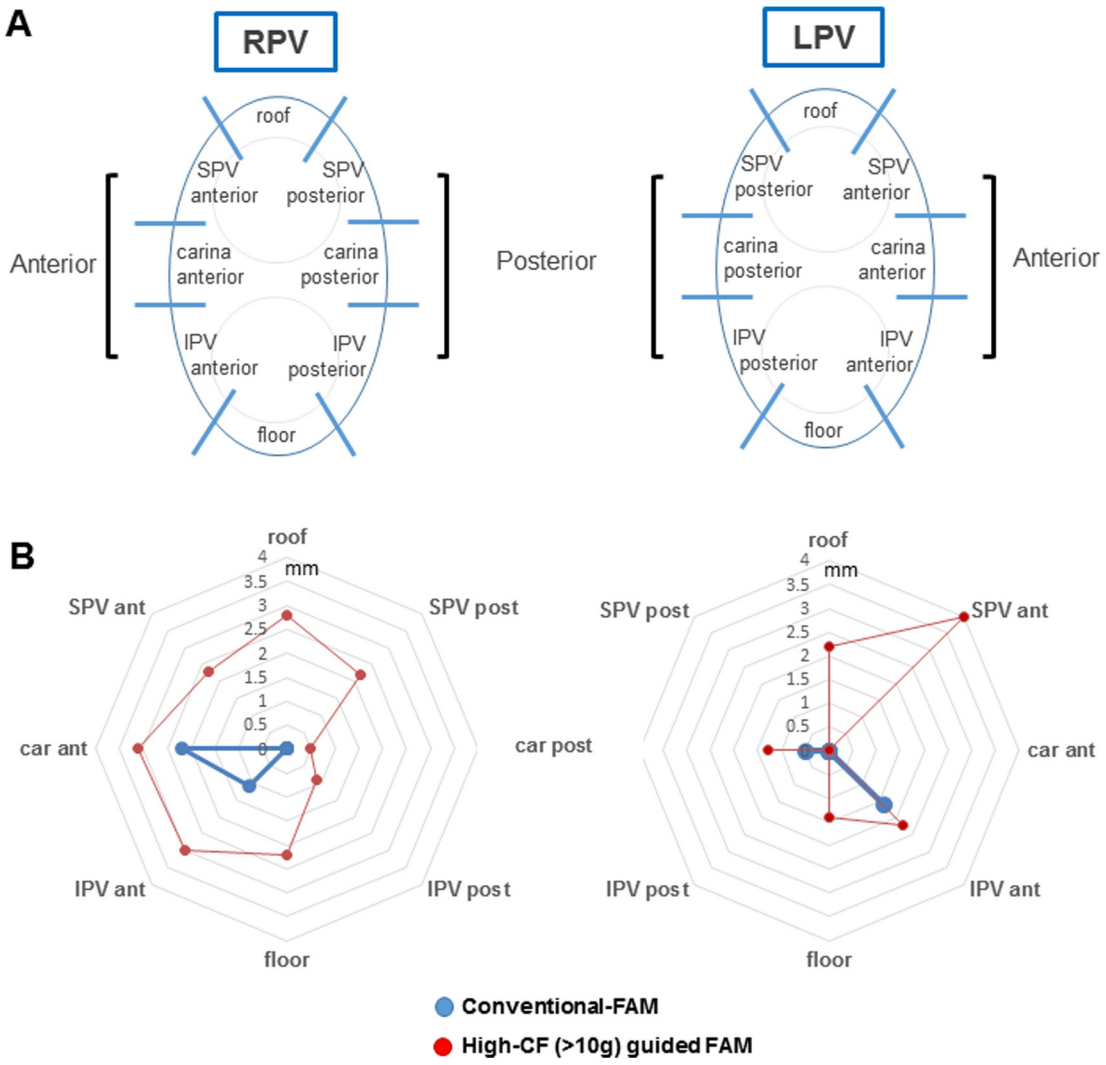


**Fig. 2.** A: Segmentation of each pulmonary vein (PV) antrum divided into 8 segments in the right and left PVs. The median shortest distance between the conventional or high CF guided FAM CF in each segment was compared between the 2 groups. B: Radar chart of the median shortest distance of each segment. SPV = left or right superior pulmonary veins; IPV = left or right inferior pulmonary veins.

The electrogram amplitude and impedance have been used as surrogates for the CF [10]. Therefore, we also evaluated the unipolar and bipolar atrial potential amplitudes and local impedance at each high-CF guided point.

### 2.6. Comparison of the high-CF guided and conventional FAM images

We measured the spatial distances between the merged 3D-CT and both the high-CF and conventional FAM derived geometries in relation to both the 16 anatomical PV locations and the 6 divided distinct LA body segments described above. In particular, we measured the shortest distance from each point to the surface depicted on the merged 3D-CT images. "Positive" values were taken to indicate mapping points located beyond the surface of the merged 3D-CT geometries. The distance of each point was averaged, and for quantification of the regional distortion of the LA, the high-CF guided FAM was compared with the conventional FAM.

### 2.7. Analysis of the contrast enhanced cardiac CT

Enhanced cardiac computed tomography (CT) of the LA has revealed 3 areas likely to be compressed by perimeter structures [11]. These are the areas from the sinus of Valsalva (non-coronary cusp) to the ascending aorta where it runs anterior to the LA and where a partially compressed area exists in the anterior wall; the area along the descending aorta that runs nearest the level of the LIPV at its antrum; and the area where the vertebrae are located posterior to the LA that is influenced by LA dilatation or vertebral distortion. The anatomical distance between those structures and any left atrial mapping point (i.e. pulmonary vein antrum and LA body region) was calculated, and any anterior or posterior external structures of <5 mm in distance from the LA anterior or posterior wall were defined as having contact (Fig. 4). In terms of the high contact force mapping around the PV antrum and LA body, we retrospectively assessed whether each map point with a high contact force (>10 g) had any contact (<5 mm) with those external structures.

### 2.8. AF ablation protocol

Circumferential pulmonary vein isolation (CPVI) was performed in the integrated 3D image using an open-irrigated ThermoCool SmartTouch catheter (Biosense Webster) in all study patients. The present catheter measures the CF based on electromagnetic location technology. RF energy was delivered at 30 W in the anterior aspect of the CPVI line and 25 W in the posterior aspect using a Stockert 70 (Biosense Webster) RF generator. The end-point of the CPVI was the elimination of all PV potentials recorded by a circular catheter (Lasso Nav, Biosense Webster) placed at the ostium of the PV, and PV-to-LA block during pacing from 10 pairs of the circular catheter at a 10-V output with 1-ms pulse width. The operator attempted to keep the CF between 10 and 20 g during the CPVI [6,12], and could check the CF using the force and direction panel, force graph, and tip display on the CARTO3 system monitor.

### 2.9. Statistical analysis

Continuous data are expressed as the mean ± standard deviation for normally distributed variables or as the median [25th, 75th percentiles] for non-normally distributed variables. The differences in the normally distributed continuous variables were analyzed by a Student t-test, and the differences in the non-normally distributed variables were analyzed by Mann–Whitney U test. Multivariate logistic regression analysis was performed to determine the predictors of a significant local distortion on the left atrial geometries. Univariate variables with a $P < 0.2$ were included in the multivariate analysis. The assumptions of the model were checked, and no significant violations were found. A probability value of a $P < 0.05$ indicated statistical significance.

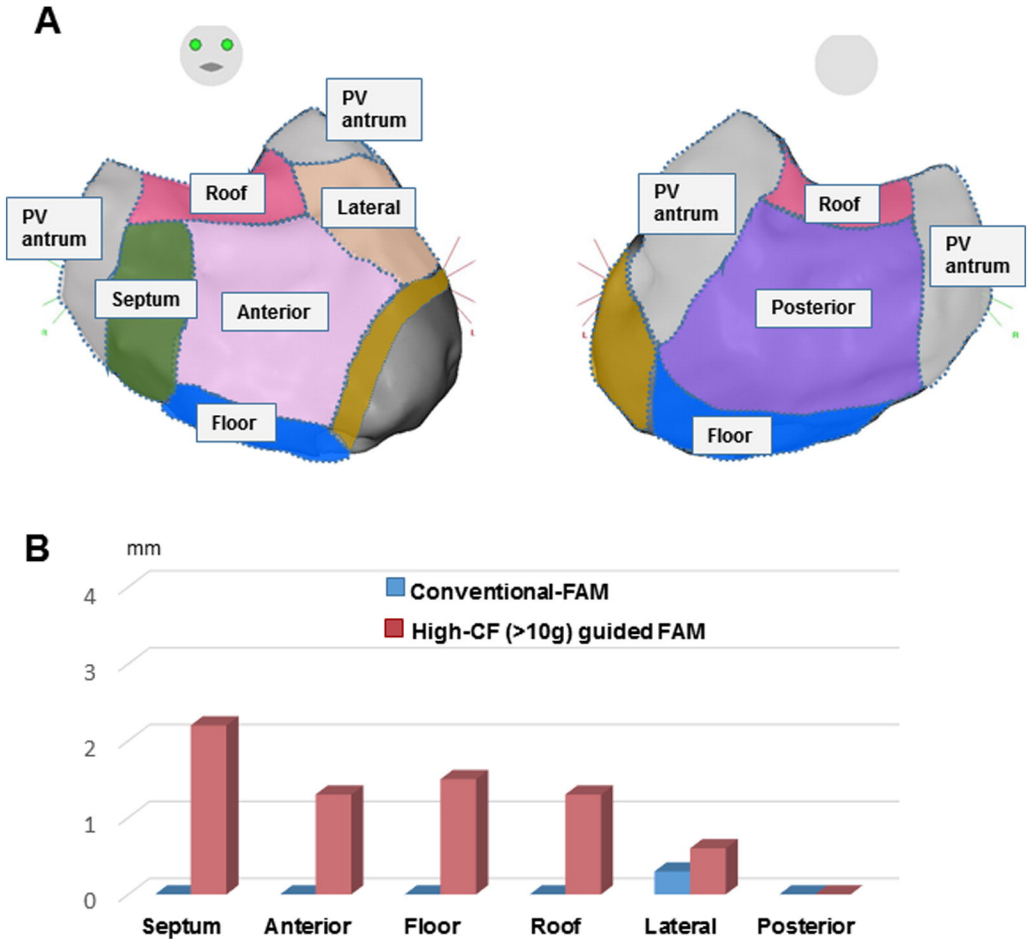


**Fig. 3.** A: Schematic of how the left atrial body region was divided regionally into 6 sections for the characterization of the anatomical distortion by the high CF guided FAM CF. B: The median shortest distance between the conventional and high CF guided FAM CF in each segment was compared between the 2 groups.

## 3. Results

### 3.1. Patient characteristics

The baseline characteristics of the patients analyzed in this study are summarized in Table 1. PVI was successfully performed in all patients. All PVs were isolated without any steam pops, however, one case had a pericardial effusion.

### 3.2. Creation of a high-CF guided FAM and conventional FAM image

Sinus rhythm was present in all patients during the entire creation of the LA geometry. A typical example of both conventional FAM and high-CF FAM images is demonstrated in Fig. 1. The total high-CF mapping points were 53 ± 2 points. The average CF was 16.0 [12.0–24.0] g at the PV antrum and 20.0 [14.9–23.7] g in the LA body region. There were no significant differences in the CF value between the left and right PV antra (16.0 [13.0–22.0] vs. 16.0 [12.0–26.0] g, P = 0.6091). The CF value in the LA body region was significantly higher than the CF in the PV antrum (20.0 [14.9–23.7] g vs. 16.0 [12.0–24.0] g, P = 0.0144).

LA volume of the conventional FAM geometries averaged 109.8 [98.2–119.3] $cm^3$ and showed no significant differences in the merged 3D-CT geometries (112 [99.3–128.5]; P = 0.4601). On the other hand, the LA volume of the high-CF derived LA geometries averaged 128.3 [112–141.3] $cm^3$ and was significantly higher than that for the conventional FAM and merged 3D-CT geometries (P < 0.05 for both).

### 3.3. Local effect of a catheter tip-derived high-CF around the PV antrum on the FAM images

Fig. 1 shows a typical example of a conventional FAM and high-CF (>10 g) guided FAM. There was no significant positive correlation between the catheter tip-tissue CF and the distorted distance from the 3D-Merge-CT geometry for both the PV antrum (r = 0.07, P = 0.30) and LA body region (r = 0.17, P = 0.21). The PV antrum distorted distance on the 3D-Merge-CT was significantly longer for the high-CF guided FAM than the conventional-FAM (1.7 [0–3.6] vs. 0 [0–1.8] mm, P < 0.0001). Fig. 2B shows the distribution of the distorted distance in the 8 segments of the right and left PVs for the high-CF and conventional-FAM groups. The regional differentiation of the distorted distance in the right PV antral region, roof (2.8 [1.1–5.6] vs. 0 [0–3.7] mm, P = 0.0074), anterior wall of both the superior (2.4 [0.8–4.2] vs. 0 [0–3.1] mm, P = 0.0201) and inferior (3.0 [0.6–6] vs. 1.1 [0–3.3] mm, P = 0.0499) PVs, and floor (2.2 [0–5] vs. 0 [0–1.7] mm, P = 0.0094) exhibited a significantly greater distortion than that for the conventional FAM. In the left PV antrum, both the anterior region (4.0 [2.1–5.6] vs. 0 [0–0.1], P < 0.0001) and roof (2.2 [0–4.4] vs. 0 [0–0], P = 0.017) of the left superior PV antrum exhibited a significantly greater distortion during the high-CF map than the conventional FAM.

Fig. 3B shows the distribution of the distorted distance in the 6 segments of the LA body region for the high-CF and conventional-FAM groups. The distorted distance in the LA body region on the 3D-Merge-CT was significantly longer for the high-CF guided FAM than conventional-FAM (1.1 [0–2.2] vs. 0 [0–0], mm P < 0.0001). The regional

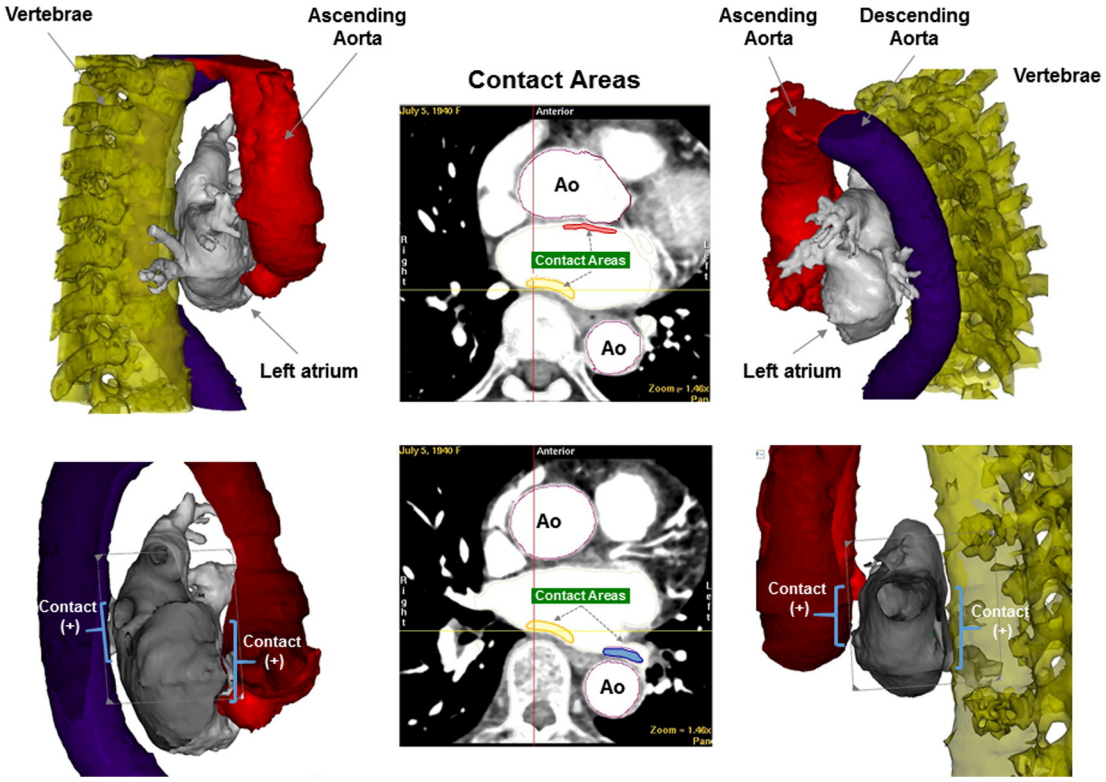


**Fig. 4.** Assessment of the left atrial contact area from the external structures including both the ascending and descending aorta and vertebrae. The anatomical distance between those structures and each mapping point, including both the pulmonary vein antrum and LA body region, was calculated. Any anterior or posterior external structures of <5 mm in distance from the LA anterior or posterior wall were defined as having contact.

differentiation of the distorted distance in the LA body region, septum (2.2 [1.2–2.8] vs. 0.1 [0–1.6] mm, P = 0.0096), anterior wall (1.3 [0–2.4] vs. 0 [0–0] mm, P = 0.0171), floor (1.6 [0.2–2.2] vs. 0 [0–0.5] mm, P = 0.004), and roof of the LA body (1.3 [0.7–3.2] vs. 0 [0–0.0] mm, P = 0.0001) exhibited a significant distortion during the high-CF map.

### 3.4. Relationship between the left anatomical contact area and local distortion

Anatomical contact areas (<5 mm) were found on the enhanced CT images in each of the 3 representative regions, the anterior (30/30 patients, 100%) and posterior (25/30 patients, 83%) left atrial regions, and LIPV antrum (28/30 patients, 93%). During high-CF guided PV antrum mapping, 10.8% (52/480) of the sites had anatomical contact (distance of <5 mm) with external structures, while 36.6% (66/180) of the sites had anatomical contact with external structures during the high-CF guided LA body mapping. In the high-CF maps, there were significant differences in the distorted distance between the regions with and without contact areas at both the PV antrum (0 [0–1.7] vs. 1.7 [0–3.99] mm, P = 0.0201) and LA body region (0 [0–1.5] vs. 1.7 [0.7–2.2] mm, P < 0.005).

We defined a significant distortion as >1.7 mm for the PV antrum and >1.1 mm for the LA body because of the median value of those measurements. In the univariate analysis, a significant distortion around the PV antrum was associated with a relatively high impedance (P = 0.0446), and the absence of contact areas (P = 0.0048). Similarly, a significant distortion in the LA body region was also associated with a relatively high impedance (P = 0.024), and absence of contact areas (P = 0.0071). A multivariate logistic regression analysis revealed that the absence of left contact areas was strongly associated with a significant local distortion in both the PV antrum (odds ratio (OR) 0.40; 95% CI, 0.17–0.97; P = 0.043) and LA body region (OR 0.28; 95% CI, 0.09–0.91; P = 0.0348), independent of the contact force and impedance (Table 2).

### 3.5. Complications

In one patient, the hospitalization was extended due to the occurrence of a pericardial effusion. In that case, an acute blood pressure drop and significant pericardial effusion emerged just after the CF guided RF application at the roof of the left superior PV. Noteworthy findings were that a significant distortion of the PV antrum was confirmed at the sites of the complication, despite having been under strict monitoring (<20 g) of the contact force (Fig. 5).

## 4. Discussion

### 4.1. Major findings

To the best of our knowledge, the present study is the first to evaluate the impact of the local left atrial distortion based on 3D-FAM-derived geometries for high CF-guided LA/PV mapping. We found that, 1) both the PV antrum and LA body distorted distance on the 3D-Merge-CT was significantly longer for high-CF guided FAM than conventional-FAM, 2) the roof of the left PV antrum, and anterior wall of the right inferior PV exhibited a significant distortion during the high-CF map, and 3) three representative left atrial contact areas with external structures were identified, and a multivariate analysis revealed that the absence of left contact areas was strongly associated with a significant local distortion on both the PV antrum and LA body region, independent of the contact force and impedance.

**Table 2**
Multivariate analysis of the significant local distortion of the left atrial geometries.

| | PV antrum | | | | Left atrial body region | | | |
|---|---|---|---|---|---|---|---|---|
| | Univariate | | Multivariate | | Univariate | | Multivariate | |
| | OR (95% CI) | P | OR (95% CI) | P | OR (95% CI) | P | OR (95% CI) | P |
| Bipolar voltage (mV) | 1.03 (0.90–1.17) | 0.66 | | | 0.75 (0.38–1.46) | 0.38 | | |
| Unipolar voltage (mV) | 1.03 (0.95–1.11) | 0.49 | | | 1.03 (0.95–1.11) | 0.51 | | |
| Impedance (Ω) | 1.01 (1.00–1.02) | 0.004 | 1.01 (0.99–1.02) | 0.101 | 1.03 (1.00–1.06) | 0.022 | 1.02 (0.99–1.05) | 0.1 |
| Contact force (g) | 1.00 (0.98–1.03) | 0.61 | | | 1.03 (0.96–1.13) | 0.36 | | |
| Absence of contact areas | 3.06 (1.35–6.91) | 0.005 | 2.46 (1.03–5.88) | 0.043 | 4.46 (1.44–13.8) | 0.007 | 3.53 (1.09–11.4) | 0.035 |

### 4.2. Impact of the high-CF on the electroanatomic geometry

In the present study, a high-CF (>10 g) altered the geometry of both the PV antrum and LA body created on electroanatomical mapping systems. As expected, the total LA volume based on the high-CF guided map was significantly more increased than that based on the conventional method. Additionally, this study showed that the local distortion derived from the high CF guided FAM differed in each segment of both the PV–LA junction and LA body region. A previous study showed that a relatively low CF (5–10 g) was the best CF for creating an LA map because the geometry was similar to the native LA [2,13]. On the other hand, a recent study recommended the guidelines based on a relatively high-CF (target 20 g, range 10–30 g) for achieving a durable PV isolation. Insufficient CF may result in an ineffective lesion, whereas excessive CF may result in complications such as a heart wall perforation, steam pop, thrombus formation, or esophageal injury [14–16]. In fact, our case demonstrated a cardiac perforation at a site with excessive distortion even while under CF monitoring. One plausible explanation for this unanticipated incident is that the RF applications to the excessively stretched atrial tissue resulted in easy penetration of the catheter tip to the epicardial aspect. Even though only one cardiac tamponade case was observed, it seems to be likely that the perforation of the atrial wall during ablation could have been caused by the balance between an excessive CF and distortion vulnerable to tissue injury. Thus, the impact of a high-CF on the local distortion of the LA geometry should be considered during PV isolation or LA substrate modification (i.e. empiric linear ablation or electrogram guided approach) procedures.

### 4.3. Impact of the external structures on the LA local distortion based on high-CF mapping

The relationship between the local anatomical distortion and value of the contact force recorded from the tip of a mapping catheter is still unclear. A prior study showed that predominant sites with a high CF (≥35 g) were observed under operator blinded mapping, especially at the rightward superior aspect of the anterior LA, which is directly beneath the ascending aorta [1]. Another study also showed the low voltage zones documented in AF patients had a relationship to the left atrial contact area, which were demonstrated in the enhanced CT [11,17]. These finding suggest that external structures surrounding the LA

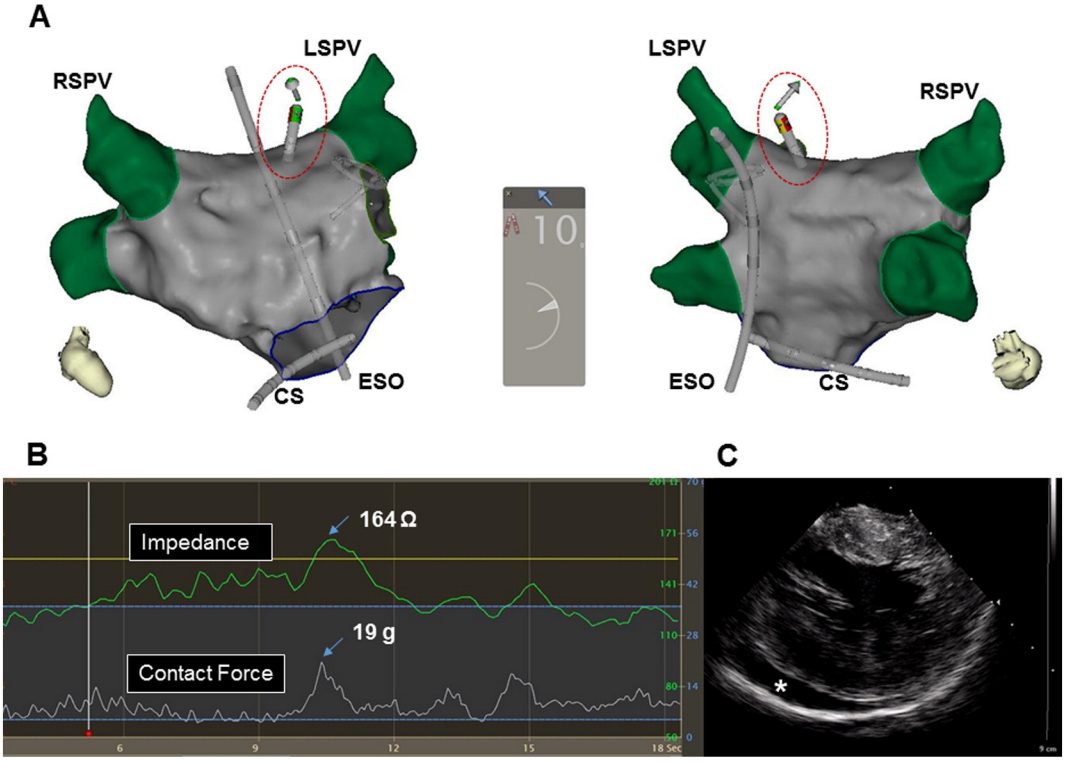


**Fig. 5.** A: Location of the ablation catheter at the site of a cardiac tamponade. Significant distortion (>1.7 mm) was documented at the roof of the left superior PV antrum. B: Temporal development of the CF and impedance during the RF application caused a pericardial effusion. A CF guided (<20 g) application was delivered, however, a sudden increase in both the CF and impedance was documented due to the patient's deep inspiration. C: Pericardial effusion, which caused a cardiac tamponade documented after the RF application with a significant catheter distortion. Pericardiocentesis was successfully performed. RF = radiofrequency.

exerts an external force against the LA and the catheter. Additionally, in the present study, no significant correlation was observed between the CF and local distortion. This finding suggests that some factors, with the exception of the contact force, are related to the cause of the excessive local distortion during high-CF guided mapping. Furthermore, a multivariate analysis demonstrated that the absence of left contact areas from external structures, independent of the local contact force, amplitude and impedance, was strongly associated with a significant local distortion of both the PV antrum and LA body region. Therefore, it seems to be likely that external structures decrease the relative distortion of the LA geometry even when under a high force contact.

Important factors to provoke a perforation of atrial tissue during ablation include the use of high power and/or high contact forces to ensure the creation of transmural lesions by RF energies. However, thinner atrial walls induced by catheter manipulation with a high-contact force also allow for a perforation to occur even more readily [18]. In the present study, a high CF was often observed adjacent to the external anatomic contact area, but the anatomical distortion at those sites was significantly smaller than other regions. Furthermore, no cardiac tamponade occurred during the mapping and ablation on those anatomical contact areas. These findings suggest that these sites may not be vulnerable to tissue damage that could result in a local perforation during the RF energy delivery. However, as the study was performed in a small number of patients, further research investigating the effect of atrial distortion on the cardiac perforative force is needed.

### *4.4. Study limitation*

This study included a relatively small cohort of patients. It should also be pointed out that there might have been slight volumetric differences in the LA geometry between the 3D-CT and FAM because the cardiac CT was performed the day before. The high-CF mapping points were a limited number of points due to the time-consuming mapping protocol during the procedure. Finally, the fluid status could partly have affected the LA geometry. However, all patients underwent the procedure under the same protocol of fasting and fluid administration in the perioperative period.

## 5. Conclusions

High-CF guided mapping yields a greater 3D-image anatomical distortion than conventional FAM methods, however, that distortion is attenuated by regions with contact areas. These findings suggest that regional anatomic distortions are involved in the existence of external structures surrounding the LA.

## Conflict of interest

None.

## Acknowledgments

We thank Mr. John Martin for his assistance in the preparation of this manuscript.

## References

[1] H. Nakagawa, J. Kautzner, A. Natale, P. Peichl, R. Cihak, D. Wichterle, et al., Locations of high contact force during left atrial mapping in atrial fibrillation patients: electrogram amplitude and impedance are poor predictors of electrode-tissue contact force for ablation of atrial fibrillation, Circ. Arrhythm. Electrophysiol. 6 (2013) 746–753.
[2] Y. Okumura, S.B. Johnson, T.J. Bunch, B.D. Henz, C.J. O'Brien, D.L. Packer, A systematical analysis of in vivo contact forces on virtual catheter tip/tissue surface contact during cardiac mapping and intervention, J. Cardiovasc. Electrophysiol. 19 (2008) 632–640.
[3] L.F. Tops, J.J. Bax, K. Zeppenfeld, M.R. Jongbloed, H.J. Lamb, E.E. van der Wall, et al., Fusion of multislice computed tomography imaging with three-dimensional electroanatomic mapping to guide radiofrequency catheter ablation procedures, Heart Rhythm. 2 (2005) 1076–1081.
[4] P.M. Kistler, K. Rajappan, M. Jahngir, M.J. Earley, S. Harris, D. Abrams, et al., The impact of CT image integration into an electroanatomic mapping system on clinical outcomes of catheter ablation of atrial fibrillation, J. Cardiovasc. Electrophysiol. 17 (2006) 1093–1101.
[5] M. Kimura, S. Sasaki, S. Owada, D. Horiuchi, K. Sasaki, T. Itoh, et al., Validation of accuracy of three-dimensional left atrial CartoSound and CT image integration: influence of respiratory phase and cardiac cycle, J. Cardiovasc. Electrophysiol. 24 (2013) 1002–1007.
[6] M. Kimura, S. Sasaki, S. Owada, D. Horiuchi, K. Sasaki, T. Itoh, et al., Comparison of lesion formation between contact force-guided and non-guided circumferential pulmonary vein isolation: a prospective, randomized study, Heart Rhythm. 11 (2014) 984–991.
[7] L. Sciarra, S. Dottori, E. De Ruvo, L. De Luca, P. Pitrone, M. Rebecchi, et al., The new electroanatomical Carto3 mapping system: three-dimensional right ventricular fast anatomical map resolution in comparison to magnetic resonance image, J. Cardiovasc. Med. (Hagerstown) 12 (2011) 434–435.
[8] M. Scaglione, L. Biasco, D. Caponi, M. Anselmino, A. Negro, P. Di Donna, et al., Visualization of multiple catheters with electroanatomical mapping reduces X-ray exposure during atrial fibrillation ablation, Europace 13 (2011) 955–962.
[9] S. Kapa, B. Desjardins, D.J. Callans, F.E. Marchlinski, S. Dixit, Contact electroanatomic mapping derived voltage criteria for characterizing left atrial scar in patients undergoing ablation for atrial fibrillation, J. Cardiovasc. Electrophysiol. 25 (2014) 1044–1052.
[10] O.J. Eick, F.H. Wittkampf, T. Bronneberg, B. Schumacher, The LETR-principle: a novel method to assess electrode-tissue contact in radiofrequency ablation, J. Cardiovasc. Electrophysiol. 9 (1998) 1180–1185.
[11] Y. Hori, S. Nakahara, T. Kamijima, N. Tsukada, A. Hayashi, S. Kobayashi, et al., Influence of left atrium anatomical contact area in persistent atrial fibrillation-relationship between low-voltage area and fractionated electrogram, Circ. J. 78 (2014) 1851–1857.
[12] K.H. Kuck, V.Y. Reddy, B. Schmidt, A. Natale, P. Neuzil, N. Saoudi, et al., A novel radiofrequency ablation catheter using contact force sensing: Toccata study, Heart Rhythm. 9 (2012) 18–23.
[13] N. Sasaki, Y. Okumura, I. Watanabe, K. Sonoda, R. Kogawa, K. Takahashi, et al., Relations between contact force, bipolar voltage amplitude, and mapping point distance from the left atrial surfaces of 3D ultrasound- and merged 3D CT-derived images: implication for atrial fibrillation mapping and ablation, Heart Rhythm. 12 (2015) 36–43.
[14] A. Thiagalingam, A. D'Avila, L. Foley, J.L. Guerrero, H. Lambert, G. Leo, et al., Importance of catheter contact force during irrigated radiofrequency ablation: evaluation in a porcine ex vivo model using a force-sensing catheter, J. Cardiovasc. Electrophysiol. 21 (2010) 806–811.
[15] J. Seiler, K.C. Roberts-Thomson, J.M. Raymond, J. Vest, E. Delacretaz, W.G. Stevenson, Steam pops during irrigated radiofrequency ablation: feasibility of impedance monitoring for prevention, Heart Rhythm. 5 (2008) 1411–1416.
[16] R. Cappato, H. Calkins, S.A. Chen, W. Davies, Y. Iesaka, J. Kalman, et al., Updated worldwide survey on the methods, efficacy, and safety of catheter ablation for human atrial fibrillation, Circ. Arrhythm. Electrophysiol. 3 (2010) 32–38.
[17] Y. Hori, S. Nakahara, N. Tsukada, A. Nakagawa, A. Hayashi, T. Komatsu, et al., The influence of the external structures in atrial fibrillation patients: relationship to focal low voltage areas in the left atrium, Int. J. Cardiol. 181 (2015) 225–231.
[18] P.G. Platonov, V. Ivanov, S.Y. Ho, L. Mitrofanova, Left atrial posterior wall thickness in patients with and without atrial fibrillation: data from 298 consecutive autopsies, J. Cardiovasc. Electrophysiol. 19 (2008) 689–692.